Available online at www.sciencedirect.com
ScienceDirect
Trans. Nonferrous Met. Soc. China 32(2022) 1019−1030
Transactions of Nonferrous Metals Society of China
www.tnmsc.cn

Spontaneous separation of Pb from $PbSO_4$-coprecipitated jarosite using freeze-thaw cycling with thiourea

Jun PENG[1*], Yang-jin WEI[1*], Mei-qing SHI[1,2], Jia-hui WU[1], Qing-wei WANG[1,2], Zhang LIN[1,2], Hui LIU[1,2], Xu YAN[1,2]

1. School of Metallurgy and Environment, Central South University, Changsha 410083, China;
2. Chinese National Engineering Research Center for Control & Treatment of Heavy Metal Pollution, Changsha 410083, China

Received 28 January 2021; accepted 26 October 2021

Abstract: To separate Pb from $PbSO_4$-coprecipitated jarosite, a novel thiourea-induced freeze-thaw cycling (T-FTC) process was investigated. Results show that distributed $PbSO_4$ particles are pressed and aggregated around the jarosite particles by T-FTC. Under the freezing-concentration effect of T-FTC, the reaction between $PbSO_4$ and thiourea is also promoted, forming lead thiourea sulfate (Pb-tu). As the cycles of T-FTC increase, $PbSO_4$ around jarosite disappears for the reaction of forming Pb-tu. After 12 cycles of T-FTC, a spontaneous separation is observed between Pb-tu and jarosite, i.e., Pb-tu is separated into the upper layer while jarosite-rich phases remain in the lower layer. Due to this spontaneous separation, leaching toxicity of the jarosite coprecipitates is reduced by 73.7%. These results suggest that T-FTC process can achieve the separation of Pb from $PbSO_4$-coprecipitated jarosite and is a promising approach for removing and recovering metals from iron-rich jarosite residues.

Key words: jarosite residues; $PbSO_4$; freeze-thaw cycling; thiourea; separation

1 Introduction

Jarosite-group minerals ($MFe_3(SO_4)_2(OH)_6$) are common iron minerals and widely found in acidic, high-sulfate environments associated with mine tailing and acid sulfate soil wetlands [1,2]. They can host various metals by adsorption, embedding, and incorporating in their structures, and such ability makes them potential scavengers for a wide range of toxic metals. Besides being ubiquitous in nature [3], jarosite-group minerals are also by-products in the metallurgical industry, for example, in the "jarosite" process of zinc hydrometallurgy, iron is removed from the hot acid-leaching liquid by precipitation as jarosite [4−6]. Meanwhile, many metals such as lead, zinc and copper are also co-precipitated along with iron upon jarosite formation [7,8]. Jarosite residues have been recognized as hazardous wastes in China due to their high toxicity. Generally, changes in environmental conditions such as pH, temperature, redox condition, and the presence of organics, may alter the behaviors of co-existed metals. Understanding the transformation of jarosite and the corresponding co-existed metals' behaviors under various conditions is worthy of consideration for both natural and industrial scenarios.

Pb is often second only to Zn as the major co-existed metals in jarosite residues, and sometimes the content of Pb exceeds that of Zn [9]. The first pathway for Pb co-existed with iron minerals is adsorption. Many previous studies indicated that Pb ions could bind strongly on the iron mineral by forming inner-sphere surface complexes [10,11]. LU et al [12] have recently

[*] Jun PENG and Yang-jin WEI contributed equally to this work

Corresponding author: Xu YAN, Tel: +86-731-88830875, Fax: +86-731-88710171, E-mail: yanxu1202@csu.edu.cn

DOI: 10.1016/S1003-6326(22)65851-5

found that Pb ions could even penetrate the loose, porous structure of hematite nano-particles by adsorption. In terms of jarosite, Pb adsorption might occur but incorporation is often more prevalent under certain conditions [13,14]. In the general chemical formula of jarosite-group minerals, Pb^{2+} could be incorporated at the M-site, forming plumbojarosite ($Pb_{0.5}Fe_3(SO_4)_2(OH)_6$) [15,16], which is the second pathway. During the formation of plumbojarosite, the formation of $PbSO_4$ is often inevitable, especially in the "jarosite" process. Several studies have found that Pb in jarosite residues is mainly in the form of $PbSO_4$ and is largely embedded by jarosite [17]. This means that embedding $PbSO_4$ in the jarosite matrix in the fast co-precipitation process is also an important pathway, even possibly dominant. Above, such multiple mechanisms for the co-existence of Pb and jarosite would contribute to complex behaviors of Pb during jarosite transformation under various conditions [18].

Freeze-thaw cycling (FTC) is a natural phenomenon that commonly happens on the earth, especially in cold areas [19,20], but its effect on the mineral structure is complex. A noticeable effect is the fragmentation of coarse mineral particles, mainly due to the volume expansion of water to form ice [21]. For porous minerals, "differential freezing effect" is another reason for mineral fragmentation to generate small particles. To be specific, when the pore water freezes, matrix water will also move to the pores, and the capillary pressure in the matrix could reduce to be negative, which may cause the extraction of small particles from the matrix. That is, freezing could enhance the mobilization of co-existed small particles into water. In the next freezing process, these colloids might be re-precipitated, attributed to a "freeze-concentration effect", i.e., they could be excluded from the ice phase and concentrated in the unfrozen regions, leading to the formation of precipitates as a result of exceeding their solubility limits [22]. In addition, freeze-concentration effect could also contribute to the acceleration of chemical reaction in frozen solution, and hence it might also promote the formation of new precipitates. Many investigations also revealed that the ice formation process is mineral species-specific and influenced by many surface attributes [23]. To our knowledge, there is no investigation about the behaviors of jarosite−Pb coprecipitates, as well as jarosite and Pb mineral, in the FTC process.

The FTC process has been reported widely for many purposes, such as fabrication of porous structures [24], food industry, and treatment of sludge/wastewater. Until now, this process has not been used to treat industrial waste. Herein, we explore the potential effect of FTC on the behavior of Pb in jarosite coprecipitates with or without a common chemical modifier, i.e. thiourea ($(NH_2)_2CS$). Thiourea has been widely used in the extraction of gold, silver and other metals. It can form complexes with metal ionic crystals through C═S bond, such as bis(thiourea) zinc chloride [25], bis(thiourea) strontium chloridethe [26], and bis(thiourea) lead chloride [27]. The following reaction explains the chemical reaction for the formation of bis(thiourea) lead chloride:

$$PbCl_2+2CS(NH_2)_2\rightarrow Pb[CS(NH_2)_2]_2Cl_2$$

In this work, we provide the first experimental evidence about the FTC influence on the co-existed metal in iron minerals (the main component of jarosite residues), and also indicate that thiourea-induced freeze-thaw cycling (T-FTC) could be a potential alternative for the treatment of jarosite residues in the future.

2 Experimental

2.1 Materials

Ferric sulfate ($Fe_2(SO_4)_3{\cdot}xH_2O$), sodium sulfate (Na_2SO_4), lead acetate ($Pb(CH_3COO)_2$), sodium hydroxide (NaOH), sulfuric acid (H_2SO_4), thiourea ($(NH_2)_2CS$) were purchased from Sinopharm Chemical Reagent Co., Ltd. (Beijing, China) and all the chemicals were of analytical-reagent grade. All solutions were prepared using ultrapure water (18 MΩ·cm).

2.2 Synthesis of jarosite, $PbSO_4$, and $PbSO_4$-coprecipitated jarosite

For the synthesis of jarosite, $Fe_2(SO_4)_3{\cdot}xH_2O$ was dissolved in the ultrapure water at 95 °C with constant stirring (400 r/min) and then 0.06 mol/L Na_2SO_4 was added until all were dissolved. The pH was adjusted to 2.0 with NaOH solution (7.0 mol/L), in which total concentration of NaOH was 0.60 mol/L. Once all the NaOH was added, the precipitates were stirred (400 r/min) for a further 3 h and then they were allowed to settle and the

residual supernatant solutions were decanted. $PbSO_4$ was synthesized using a 1 L solution containing 0.1 mol/L $Pb(CH_3COO)_2$ and 0.1 mol/L H_2SO_4, while all were dissolved at room temperature with constant stirring (300 r/min). $PbSO_4$-coprecipitated jarosite was synthesized using a 1 L solution containing 0.25 mol/L $Fe_2(SO_4)_3{\cdot}xH_2O$ and 0.06 mol/L Na_2SO_4 at 95 °C with constant stirring (600 r/min). The pH was adjusted to 1.0 with NaOH solution (7.0 mol/L) and then 100 mL of 0.3 mol/L $Pb(CH_3COO)_2$ solution was added at a rate of 50 mL/h under stirring, meanwhile, NaOH solution was added until the pH was adjusted to 2.0, then the precipitates were stirred (600 r/min) for a further 3 h, after which they were allowed to settle and the residual supernatant solutions were decanted. After the synthesis, the jarosite, $PbSO_4$, and $PbSO_4$-coprecipitated jarosite were separated from solution by centrifugation, washed several times with ultrapure water (18 MΩ·cm), and then dried at 80 °C for 24 h.

2.3 Procedure of T-FTC

The suspension was prepared by adding 1 g of different samples (i.e. jarosite, $PbSO_4$ or $PbSO_4$-coprecipitated jarosite) and 2 g thiourea into 50 mL of ultrapure water in conical tubes and then sonicated for 2 min for better dispersion, the pH value of solution was kept at 6.0−6.3. For the FTC process, the conical tubes were placed in a laboratory refrigerator at −20 °C for 12 h for freezing the suspension. After freezing, the conical tubes were placed in a beaker containing lukewarm water (20 °C) for thawing. The sample suspension was frozen from 20 to −20 °C for 12 h and then thawed at 20 °C for one cycle and freeze-thaw cycle was performed 0−12 cycles by repeating the above procedure. Moreover, FTC experiment and thiourea reaction experiment were conducted. FTC experiment procedures were the same as T-FTC experiment but without adding thiourea. Thiourea reaction experiment was conducted by putting different samples and 2 g thiourea into ultrapure deionized water (50 mL), then the temperature was kept at 20 °C for the same time compared with FTC or T-FTC. All the samples were separated from solution by centrifugation, washed several times with ultrapure water (18 MΩ·cm), and then dried at 80 °C for 24 h.

2.4 Analysis methods

The microstructure and surface morphology were observed by scanning electron microscope (SEM, Japan Hitachi Ltd). The phase composition was analyzed by X-ray diffractometer (XRD, Bruker AXS, Germany) with a graphite monochromator using Cu K_α radiation with a 2θ range of 5°−80° using 0.01° steps with 28.8 s of integration time per step under operating conditions of 40 kV and 40 mA. The functional groups of different solid samples were distinguished by Fourier transformed infrared spectroscope (FTIR, NicoletIS10, USA) in the 4000−400 cm^{-1} spectral range with 32 scans per spectrum at a resolution of 4 cm^{-1}. The leaching toxicity experiment was based on sulphuric acid and nitric acid method (HJ/T 299—2007).

3 Results and discussion

3.1 Structural stability of jarosite during T-FTC

Figure 1 presents XRD patterns and SEM images of jarosite after different treatments. As seen in Fig. 1(a), the XRD peaks are narrow and strong, and all well match to those of natrojarosite (PDF No. 36-0425), confirming that the synthesized solid is highly crystal natrojarosite. No additional peak is detected, suggesting that no compound is present at a detectable level. XRD patterns of natrojarosite after FTC and T-FTC also show no difference. The SEM image (Fig. 1(b)) of synthesized natrojarosite shows well-defined, uniform, and rhombohedral crystals with smooth surfaces, which were also reported in other studies [28]. Besides, the particle size is homogeneous in the range of 3−10 μm. Such highly crystalline and large size natrojarosite is potential for good solid−liquid separation, which is the main reason for its use in zinc hydrometallurgy instead of $Fe(OH)_3$. In addition, it can be found that the morphology of natrojarosite shows no difference after FTC (Fig. 1(c)) or T-FTC (Fig. 1(d)), and the integrality of jarosite is still evident. The XRD and SEM data reveal the structural stability of jarosite after FTC and T-FTC.

Such structural stability of jarosite during T-FTC is possibly related to the mechanism of FTC. As mentioned above, the main influence of FTC on solid structure involves fragmentation, enhanced aggregation and re-precipitation, and acceleration of chemical reaction due to freeze-concentration effect [29]. For fragmentation mechanism, porous

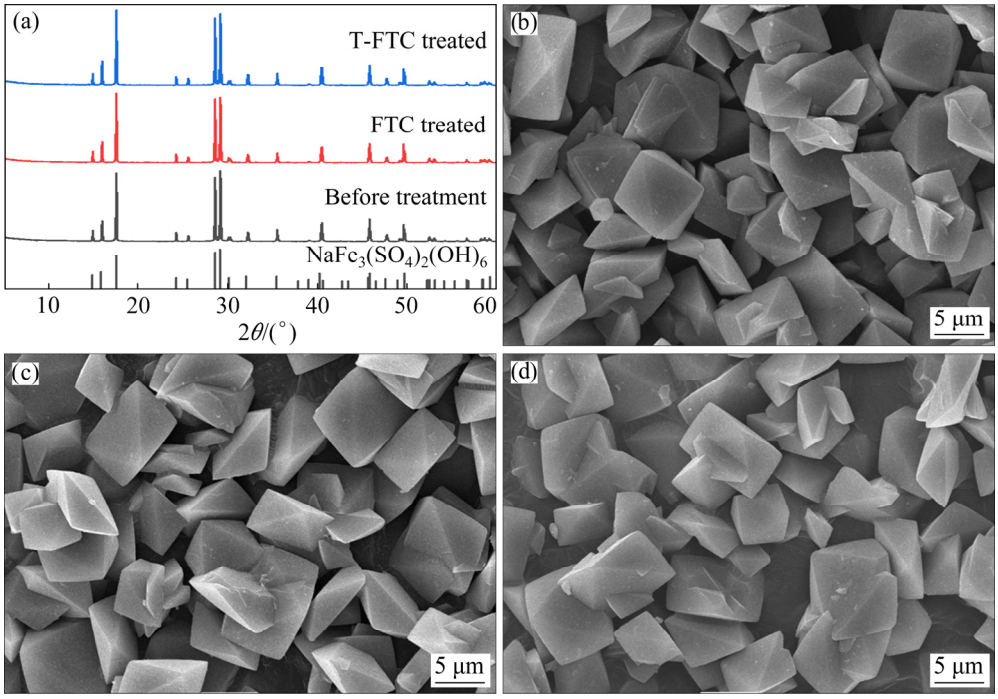

Fig. 1 XRD patterns (a) and SEM images (b−d) of synthesized jarosite treated under different conditions: (b) Before treatment; (c) FTC treated; (d) T-FTC treated (Before treatment: Without any treatment; FTC treated: Treated by freeze-thaw cycling only; Thiourea treated: Treated at 20 °C by thiourea only; T-FTC treated: Treated by thiourea-induced freeze-thaw cycling)

structures or rugged surfaces are often necessary. Its effect on minerals with smooth surfaces and high crystallinity (such as natrojarosite synthesized here) would be weaker. In the cases of enhanced aggregation and re-precipitation, small particles are usually more susceptible than large particles. Here, the size of natrojarosite is as high as several micrometers, and hence the effect of enhanced aggregation and re-precipitation is difficult to function. Moreover, there is no chemical reaction between natrojarosite and thiourea, corresponding to no aggregation effect. Overall, the integrality of jarosite crystals is maintained during T-FTC.

3.2 Aggregation and transformation of $PbSO_4$ during T-FTC

$PbSO_4$ is the dominant form of lead in jarosite residues [17]. Here, the effect of T-FTC on $PbSO_4$ was investigated. XRD patterns show that the synthesized $PbSO_4$ has high crystallinity (Fig. 2). SEM images (Figs. 3(a, c)) show clearly granular-shaped $PbSO_4$, which is similar to the commercial $PbSO_4$, but the size of the synthesized $PbSO_4$ is smaller (0.5−1.0 μm). Compared to micron-sized natrojarosite, the submicron-sized $PbSO_4$ particle

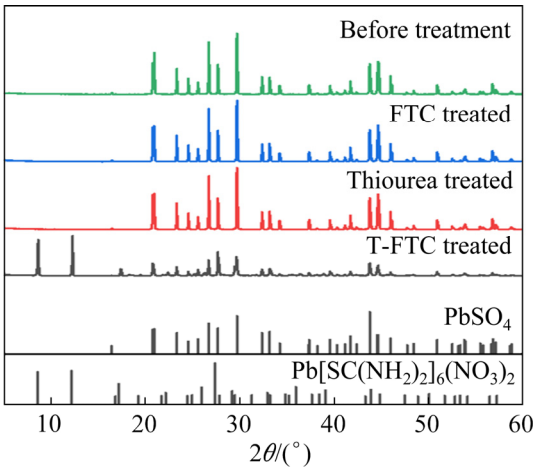

Fig. 2 XRD patterns of synthesized $PbSO_4$ treated under different conditions

might be more sensitive to freeze-concentration effect. After FTC, the XRD patterns of $PbSO_4$ show no apparent difference. However, the SEM image (Fig. 3(d)) reveals intuitive morphological changes that occurred after 12 cycles of FTC, i.e. not only the aggregation of the particles, but also the fusion of particles to be larger after FTC. We speculate that although no chemical agent is added, $PbSO_4$ particles could be coalesced rather than simple

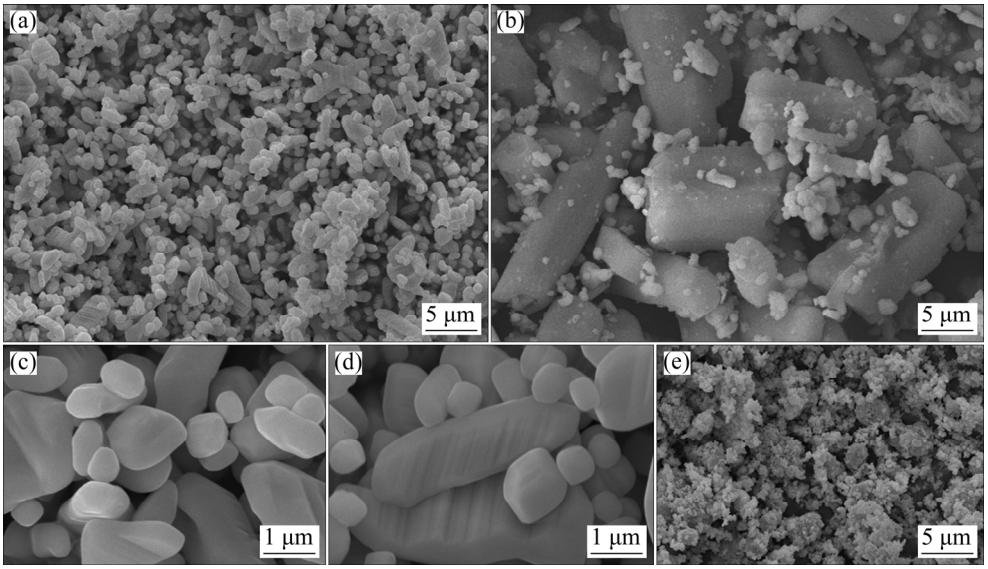

Fig. 3 SEM images of synthesized $PbSO_4$: (a, c) Before treatment; (b) T-FTC treated; (d) FTC treated; (e) Thiourea treated

aggregation during FTC. Moreover, the effect of thiourea addition on $PbSO_4$ without FTC was investigated. From the SEM image in Fig. 3(e), there are many irregular particles with sizes in tens of nanometers appearing around the $PbSO_4$ substrate. XRD results show a large decrease in $PbSO_4$ peak intensity compared to synthesized $PbSO_4$, consistent with the amorphization of $PbSO_4$, as shown in the SEM image. No new peak is detected, suggesting that the reaction product is too few to be detected by XRD or it is amorphous.

After T-FTC, a clear morphological and structural change in the $PbSO_4$ particles can be seen. The SEM image (Fig. 3(b)) indicates the formation of elongated crystals in the $PbSO_4$ substrate. Obviously, the size of the new crystals significantly increases. The EDS analysis (Fig. 4) on a single particle confirms the presence of Pb, S, C, N and O in a molar ratio of 1:7.6:9.8:19.4:6.7, implying the formation of $Pb[SC(NH_2)_2]_6SO_4$. XRD pattern of $PbSO_4$ after T-FTC shows that peaks around 2θ=8.58° and 11.21° clearly appear, attributed to the formation of some new phases. These new peaks are strong and narrow, revealing a good crystallinity of the products. The crystal structure of this new phase is similar to lead thiourea nitrate ($Pb[SC(NH_2)_2]_6(NO_3)_2$, PDF No. 00-054-0300).

Taken together, the XRD and SEM−EDS data are consistent and demonstrate that lead thiourea sulfate (hereafter Pb-tu) with high crystallinity and large size is formed after T-FTC. As reported, this

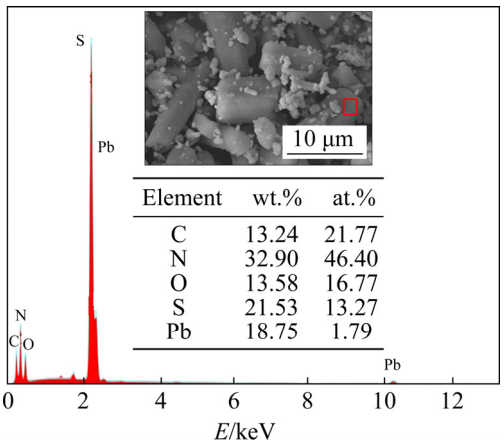

Fig. 4 SEM−EDS results of $PbSO_4$ after T-FTC treatment

kind of new phase is a polymeric semi-organic nonlinear optical crystal, where thiourea is ionically bonded to the metal ions [30]. But it is uncommon and has not been observed in other conditions. Here, the easy formation of Pb-tu proves the acceleration effect of FTC on a certain chemical reaction, which has been found in some previous studies [31,32].

3.3 Spontaneous separation of Pb from $PbSO_4$-coprecipitated jarosite by T-FTC

Figure 5 presents the SEM and XRD results of synthesized $PbSO_4$-coprecipitated jarosite. In the XRD patterns (Fig. 5(a)), natrojarosite is still observed to be the major phase of the co-precipitates, while $PbSO_4$ peaks are clearly observed at 2θ=20.90°, 29.68°, and 43.75°, which

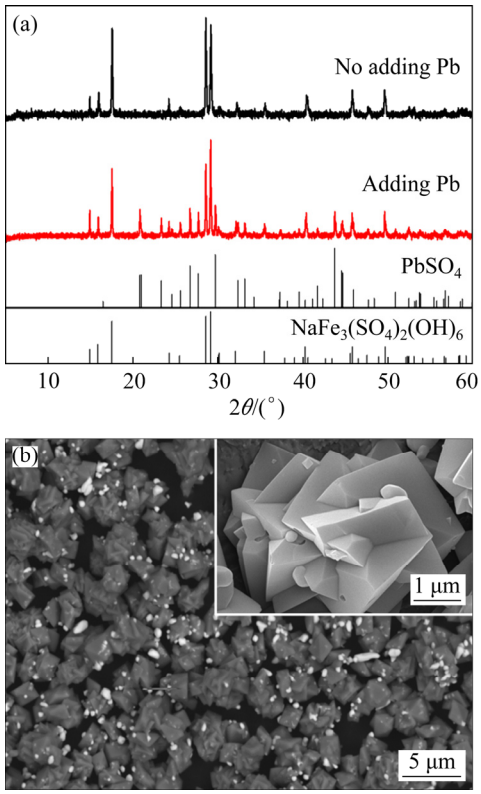

Fig. 5 XRD patterns (a) and SEM images (b) of $PbSO_4$-coprecipitated jarosite

confirms the formation of $PbSO_4$ along with natrojarosite. The SEM−BSE images (Fig. 5(b)) of samples are taken to show the difference of chemical compositions in the sample. Clearly, the co-precipitates are two-phase. They consist of ~10 μm darker particles and ~1 μm brighter grains. SEM−EDS analysis shows the major elements of darker phase containing Na, Fe, S, and O in a molar ratio of 1:4.6:2.2:17.0, i.e. natrojarosite (Fig. 6(b)), while the brighter particles contain Pb, S, and O in a molar ratio of 1:0.9:3.9, i.e. $PbSO_4$ (Fig. 6(c)). Notably, the small $PbSO_4$ particles are widely distributed in the jarosite substrate. The inset in SEM image in Fig. 5(b) shows that the synthesized $PbSO_4$-precipitated jarosite also has pseudo-rhombohedral morphology, but it is changed to be intergrown due to the introduction of $PbSO_4$. Such an intergrown structure could provide convenience for the fragmentation mechanism of FTC. We expect that these distributed and tiny $PbSO_4$ particles in natrojarosite substrate could largely transform during T-FTC based on above results.

It was surprisingly found that a spontaneous separation phenomenon was observed when $PbSO_4$-

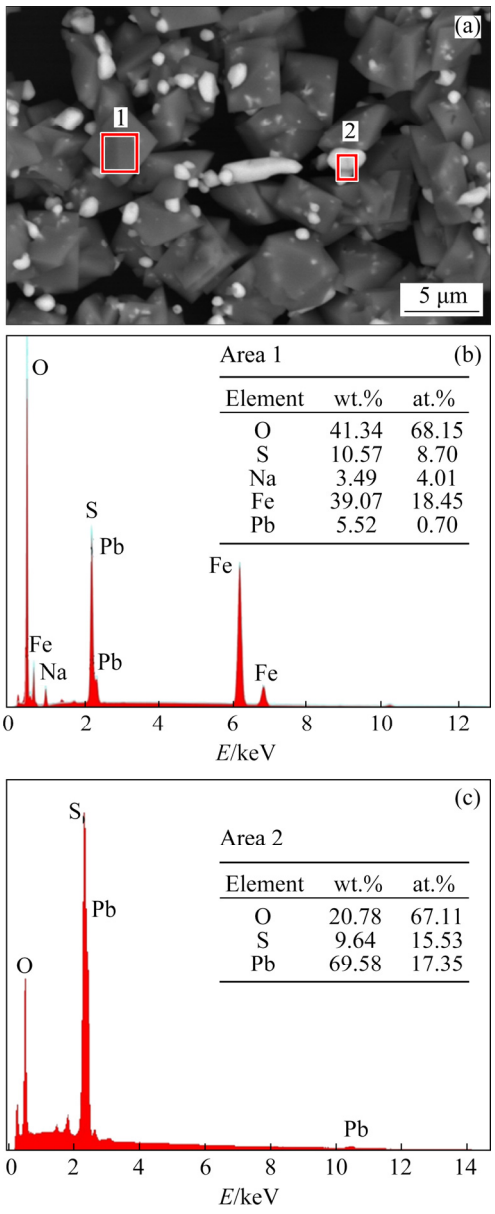

Fig. 6 SEM image (a) and SEM−EDS data (b, c) of $PbSO_4$-coprecipitated jarosite

coprecipitated jarosite was treated by 12 cycles of T-FTC. Initially, the $PbSO_4$-coprecipitated jarosite was well mixed in solution (Fig. 7(a)). After 12 cycles of T-FTC, the homogeneous mixture was spontaneously separated into the upper white solid and lower jarosite-rich phases (Fig. 7(c)). As the 12th thawing proceeded, the upper layer gradually thinned until it disappeared (Fig. 7(d)), possibly due to the gradual dissolution of white solid into solution. Then, the completely dissolved upper solution was separated and collected. It is interesting to note that some white rod-like precipitates were formed readily in the solution after cooling down the collected solution below

4 °C again (Fig. 7(e)). We speculated these white solids separated from co-precipitates were Pb-containing matters.

The white rod-like precipitates were collected and characterized by SEM and XRD. SEM image (Fig. 8(a)) shows that their structural features are similar to those observed in Fig. 3(b), and the results obtained by SEM−EDS (Fig. 8(b)) show the presence of Pb and S with similar Pb/S molar ratio (1:6.5). As further confirmed by the XRD pattern (Fig. 8(c)), all of the diffraction peaks are well-indexed to the lead thiourea nitrate, which supports the formation of pure "lead thiourea-type" matter. Lastly, the white solids were characterized using FTIR and thiourea as comparison (Fig. 9). It could be seen that the absorption peak corresponding to $\delta(NH_2)$ at 1633.12 cm^{-1} disappears, and the peak related to N—C—N vibrations in the thiourea group at 1093.16 cm^{-1} is broadened after T-FTC. The FTIR results are possibly attributed that Pb is bound to thiourea.

The main aim of controlling and separating Pb is to reduce the environmental risk of residues, so the leaching toxicity of coprecipitates was analyzed. It can be found that the leaching toxicity of T-FTC treated samples (Pb, 19.43 mg/L) is much lower than that of the original samples (Pb, 73.91 mg/L). Leaching toxicity of the jarosite coprecipitates is reduced by 73.7%, indicating a significant reduction in the environmental toxicity. The above results suggest that T-FTC is a promising approach for removing and recovering metals from iron-rich jarosite residues.

3.4 Mechanism of Pb separation

To understand the T-FTC process mechanism for $PbSO_4$-coprecipitated jarosite, samples treated by FTC and thiourea process were collected as controls, and the SEM and XRD results are shown in Fig. 10 and Fig. 11, respectively. As seen in SEM images (Figs. 10(a, b)), the $PbSO_4$ phase is still widely dispersed in the jarosite matrix after FTC treatment, indicating that the effect of FTC on the transformation of $PbSO_4$ is limited. As for thiourea treatment, the aggregation of $PbSO_4$ is evident, as shown in Figs. 10(c, d).

The XRD patterns (Fig. 11) show that the main phases of both samples are natrojarosite and $PbSO_4$. No pronounced diffraction peak of Pb-tu is detected, possibly because the reaction process between $PbSO_4$ and thiourea is not significant (for FTC process), or the new-formed Pb-tu is not of high crystallization (for thiourea process), which are consistent with the above results.

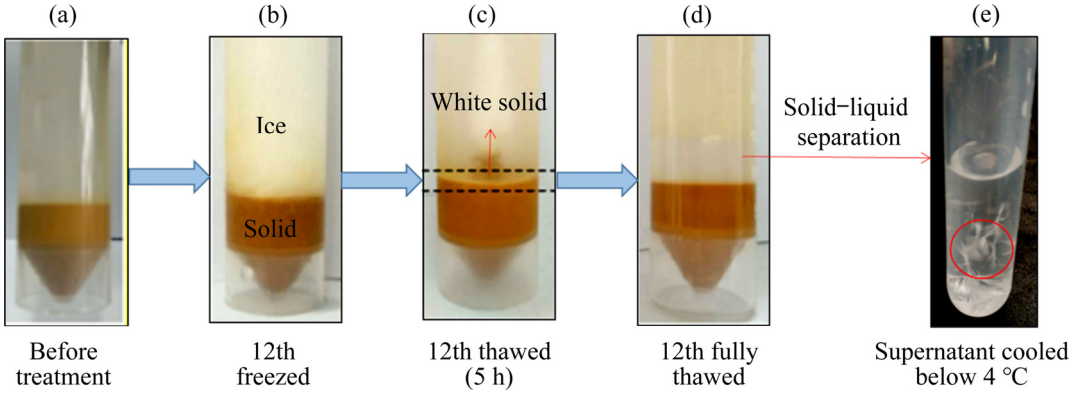

Fig. 7 Separation process of $PbSO_4$-coprecipitated jarosite

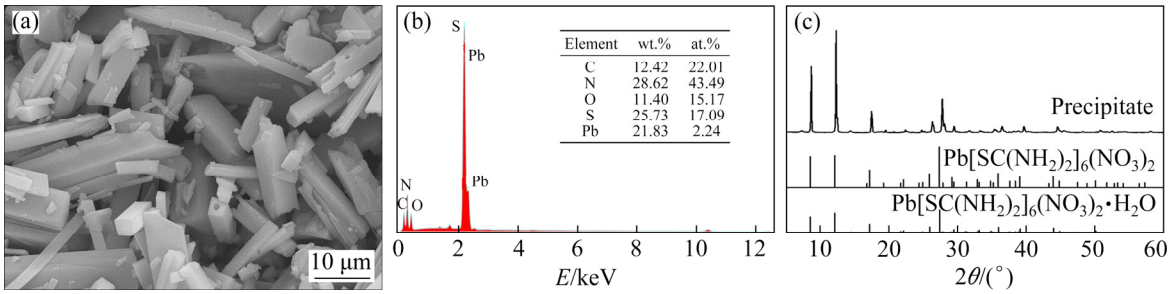

Fig. 8 Analysis of white rod-like precipitates: (a) SEM image; (b) EDS results; (c) XRD patterns

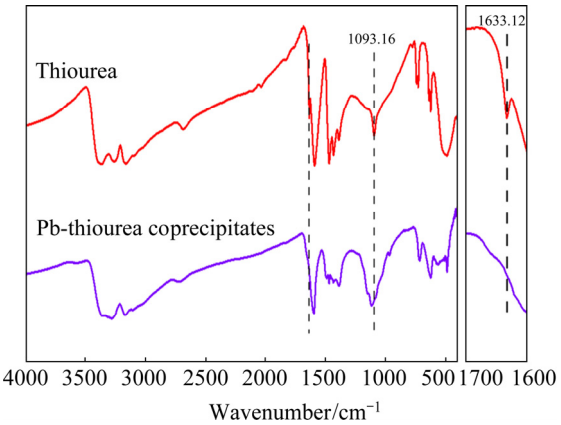

Fig. 9 FTIR analysis of thiourea and Pb-thiourea coprecipitates

Figure 12 displays the SEM images of $PbSO_4$-coprecipitated jarosite samples treated after different cycles of T-FTC. Unlike the wide dispersion of $PbSO_4$ particles in the jarosite substrate, the local aggregation of Pb-containing particles after T-FTC is apparent. Specifically, as the cycles of T-FTC increased (Figs. 12(b, c)), the distributed $PbSO_4$ particles in coprecipitates are gradually aggregated. As seen in the enlarged view (Fig. 12(e)), the morphology of $PbSO_4$ changes into sheets and is closely aggregated around the jarosite particles. The effect of aggregation described here is consistent with previous studies on FTC [33]. After 12 cycles of T-FTC, no obvious lighter phase is detected in the SEM image, implying the dissolution of Pb-containing aggregates from the natrojarosite matrix as the reaction between $PbSO_4$ and thiourea is significant and completely finished. The surface cavity of the jarosite matrix may be caused by this fragmentation effect or the reaction between thiourea and $PbSO_4$ embedded in the jarosite surface (Fig. 12(d)).

Changes in the mineralogy of samples were also examined via XRD analysis. As seen in Fig. 13, the natrojarosite structure in the coprecipitates remains stable during T-FTC, even after many cycles. Small diffraction peaks (2θ=20.90°, 29.68°, 43.75°) of crystal plane of $PbSO_4$ are present at initial, but their intensity decreases gradually with increasing the cycle number. It is possibly attributed to the dissolution of $PbSO_4$ as the process progresses. To verify this, we also monitored the concentration of total Pb^{2+} and SO_4^{2-} in the solution after every thawing operation during the 12-cycle T-FTC process. Results show that the concentrations of both total Pb^{2+} and SO_4^{2-} increase with the increase of cycles and their change trends are basically the same, indicating the gradual dissolution of $PbSO_4$. In addition, Fig. 13 shows that there are still some weak diffraction peaks of $PbSO_4$ after 12 cycles, which indicates that $PbSO_4$

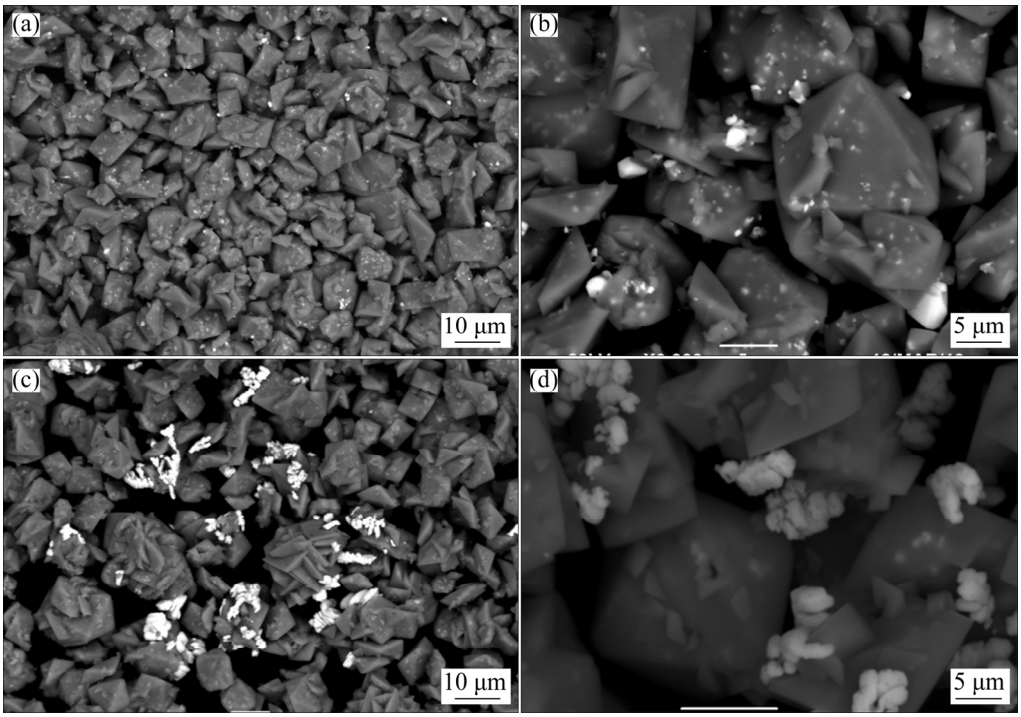

Fig. 10 SEM images of $PbSO_4$-coprecipitated jarosite: (a, b) FTC treated; (c, d) Thiourea treated

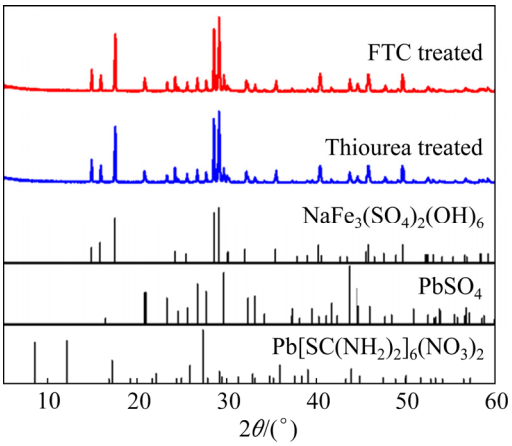

Fig. 11 XRD patterns of $PbSO_4$-coprecipitated jarosite

has not been removed completely. For this point, we expect that the remaining $PbSO_4$ can be further removed by increasing the freezing-thawing cycles.

Further study on the optimization of the conditions is currently under investigation.

Based on the above results, a possible mechanism of T-FTC on the spontaneous separation of Pb from $PbSO_4$-coprecipitated jarosite was proposed, and its schematic diagram is presented in Fig. 14. In the initial cycles, distributed $PbSO_4$ particles can be pushed by the crystallization front as the ice crystallization. With ice crystal growing, concentrated $PbSO_4$ particles are confined in the unfrozen solution surrounded by walls of ice grains and natrojarosite matrix. As ice crystals grow, $PbSO_4$ particles are much more concentrated because they cannot escape from the solution surrounded by the walls and are also difficultly incorporated into the ice grains. As a result, the $PbSO_4$ particles are pressed on the surface of natrojarosite, and their morphology is changed into

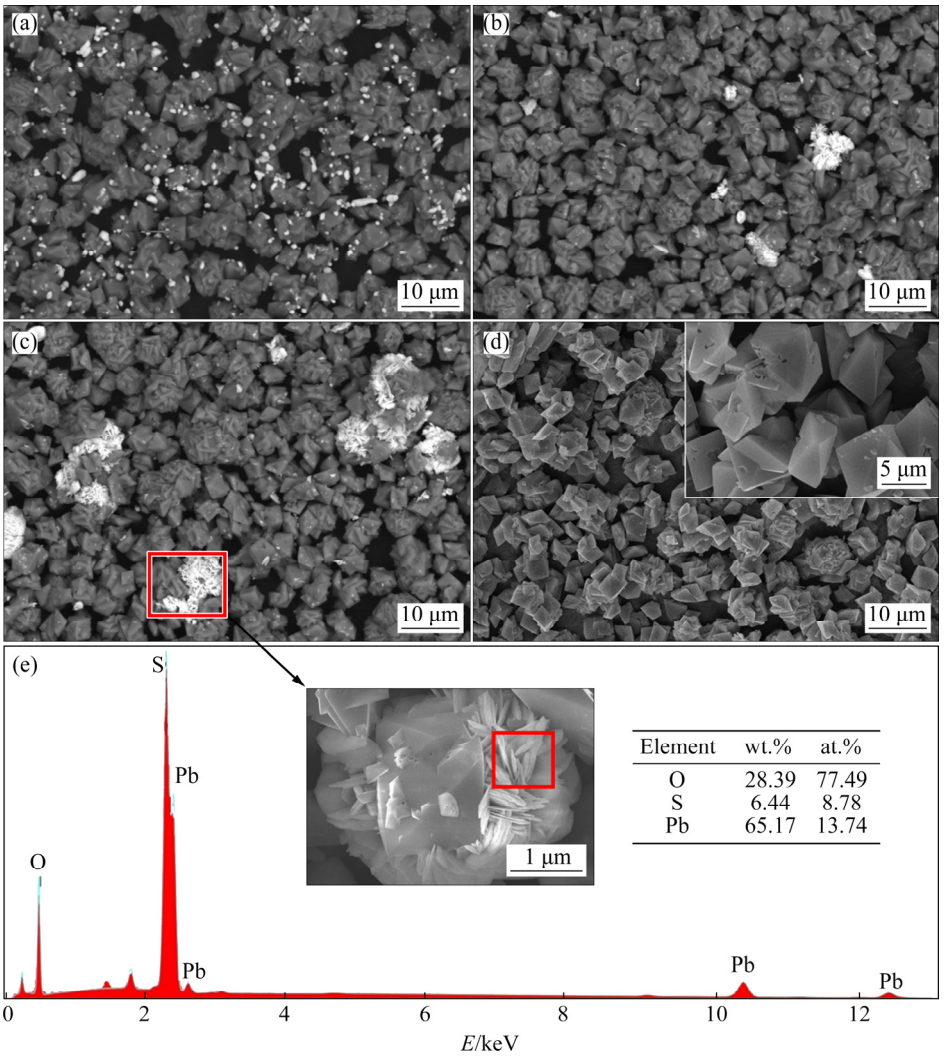

Fig. 12 SEM images (a−d) and SEM−EDS results (e) of $PbSO_4$-coprecipitated jarosite after different cycles of T-FTC: (a) 0 cycle; (b) 3 cycles; (c, e) 6 cycles; (d) 12 cycles

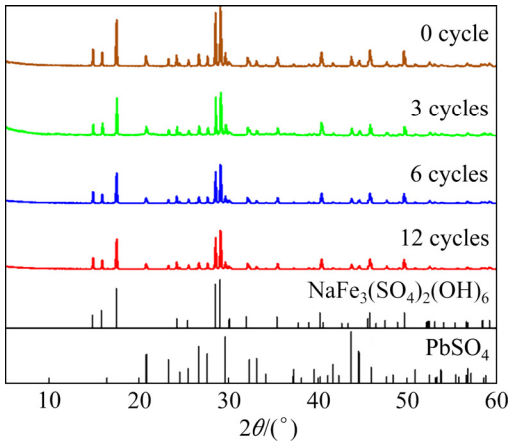

Fig. 13 XRD patterns of $PbSO_4$-coprecipitated jarosite after different cycles of T-FTC

sheets. Such a surface aggregation phenomenon was also observed by GERMAN et al [34]. During thawing, there can be a maturation process, where the larger $PbSO_4$ crystals grow in size at the expense of dissolving the smaller particles. Above, the aggregation and maturation processes lead to the formation of large $PbSO_4$ particles, as shown in Figs. 12(b, c).

As T-FTC cycles increase further, the $PbSO_4$ particles are highly aggregated and could be easily reacted with thiourea, whose concentration is also extremely high in the confined solution due to the "freeze-concentration" effect derived from FTC [35,36]. Some small $PbSO_4$ particles can react and disappear quickly, while $PbSO_4$ particles with larger size must experience a sufficient number of T-FTC cycles before they disappear completely. Here, 12 cycles, and perhaps even more cycles of FTC are needed for the large $PbSO_4$ to be reacted completely. Meanwhile, as the small $PbSO_4$ particles dissolve as mentioned above, a small amount of Pb^{2+} and SO_4^{2-} will be released in the solution. The Pb^{2+} could also react with thiourea to form Pb-tu. Once Pb-tu forms, the separation of Pb-tu and jarosite will not be difficult. Pb-tu is more soluble in the solution, and thus Pb-tu can be collected by solid−liquid separation during the thawing process. The Pb-tu solid can be further recrystallized by cooling the solution again, and finally the separation of $PbSO_4$ and jarosite is realized.

4 Conclusions

(1) During the T-FTC treatment, $PbSO_4$ was pressed and aggregated around the jarosite substrate. The reaction between $PbSO_4$ and thiourea was significantly promoted to form Pb-tu during T-FTC while the reaction rate was very slow at 20 °C. These phenomena were possibly due to the freeze-concentration effect and the fragmentation effect of FTC.

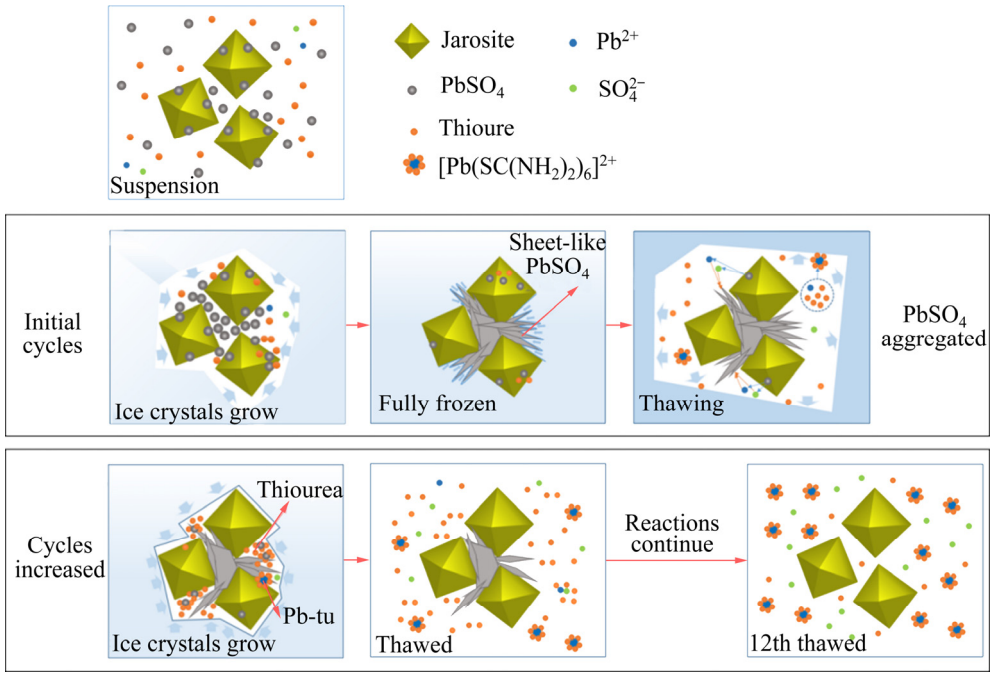

Fig. 14 Schematic illustration of mechanism of T-FTC process for Pb separation from $PbSO_4$-coprecipitated jarosite

(2) As the cycles of T-FTC increased, $PbSO_4$ was dissolved and transformed to Pb-tu for the reaction between $PbSO_4$ and thiourea. After 12 cycles of T-FTC, a spontaneous separation was observed between new-formed Pb-tu and jarosite, i.e. Pb-tu was separated into the upper layer while jarosite-rich phases remained lower layer.

(3) As a result, the leaching toxicity of the jarosite coprecipitates was reduced by 73.7% (from 73.91 mg/L to 19.43 mg/L). Further research should be carried out to reduce leaching toxicity further by optimizing the conditions or combining with other methods.

Acknowledgments

This work was financially supported by the National Natural Science Foundation of China (Nos. 51904355, 51825403), and the National Key R&D Program of China (No. 2020YFC1909201).

References

[1] CRABBE H, FERNANDEZ N, JONES F. Crystallization of jarosite in the presence of amino acids [J]. Journal of Crystal Growth, 2015, 416: 28−33.

[2] NIE Zhen-yuan, ZHANG Wei-wei, LIU Hong-chang, ZHU Hong-rui, ZHAO Chang-hui, ZHANG Duo-rui, ZHU Wei, MA Chen-yan, XIA Jin-lan. Bioleaching of chalcopyrite with different crystal phases by *Acidianus manzaensis* [J]. Transactions of Nonferrous Metals Society of China, 2019, 29(3): 617−624.

[3] LI Hai-jun, YANG Hong-ying, CHEN Guo-bao. Catalytic performance of biological method seeds on jarosite process [J]. Transactions of Nonferrous Metals Society of China, 2016, 26(2): 557−564.

[4] LIU Peng-fei, ZHANG Yi-fei, WANG Li, YOU Shao-wei, BO Jing. Thermodynamics and nucleation mechanism of ammonium jarosite in sulfuric acid solution [J]. Journal of Crystal Growth, 2017, 478: 52−57.

[5] DENG Zhi-gan, YANG Fan, WEI Chang, ZHU Bei-ping, ZENG Peng, LI Xing-bin, LI Cun-xiong, LI Min-ting. Transformation behavior of ferrous sulfate during hematite precipitation for iron removal [J]. Transactions of Nonferrous Metals Society of China, 2020, 30(2): 492−500.

[6] JIA Li-pan, HUANG Jiang-jiang, MA Ze-long, LIU Xu-heng, CHEN Xing-yu, LI Jiang-tao, HE Li-hua, ZHAO Zhong-wei. Research and development trends of hydrometallurgy: An overview based on hydrometallurgy literature from 1975 to 2019 [J]. Transactions of Nonferrous Metals Society of China, 2020, 30(11): 3147−3160.

[7] BEDI A, SINGH B R, DESHMUKH S K, AGGARWAL N, BARROW C J, ADHOLEYA A. Development of a novel myconanomining approach for the recovery of agriculturally important elements from jarosite waste [J]. Journal of Environmental Sciences, 2018, 67: 356−367.

[8] LOU Xiao-ming, ZHANG You-xiang. Synthesis of $LiFePO_4$/C cathode materials with both high-rate capability and high tap density for lithium-ion batteries [J]. Journal of Materials Chemistry, 2011, 21(12): 4156−4160.

[9] HAN Hai-sheng, SUN Wei, HU Yue-hua, JIA Bao-liang, TANG Hong-hu. Anglesite and silver recovery from jarosite residues through roasting and sulfidization−flotation in zinc hydrometallurgy [J]. Journal of Hazardous Materials, 2014, 278(15): 49−54.

[10] OSTERGREN J D, BROWN G E, PARKS G A, PERSSON P. Inorganic ligand effects on Pb(II) sorption to goethite (α-FeOOH): II. Sulfate [J]. Journal of Colloid and Interface Science, 2000, 225(2): 483−493.

[11] YAN Hong-jie, ZHANG He-yang, SHI Ya-jun, ZHOU Ping, LI Huan, WU Dong-ling, LIU Liu. Simulation on release of heavy metals Cd and Pb in sediments [J]. Transactions of Nonferrous Metals Society of China, 2021, 31(1): 277−287.

[12] LU Yang, HU Shi-wen, WANG Zi-meng, DING Yang, LU Gui-ning, LIN Zhang, DANG Zhi, SHI Zhen-qing. Ferrihydrite transformation under the impact of humic acid and Pb: Kinetics, nanoscale mechanisms, and implications for C and Pb dynamics [J]. Environmental Science: Nano, 2019, 6: 747−762.

[13] PALDEN T, REGADÍO M, ONGHENA B, BINNEMANS K. Selective metal recovery from jarosite residue by leaching with acid-equilibrated ionic liquids and precipitation-stripping [J]. ACS Sustainable Chemistry & Engineering, 2019, 7(4): 4239−4246.

[14] AGUILAR-CARRILLO J, VILLALOBOS M, PI-PUIG T, ESCOBAR-QUIROZ I N, ROMERO F M. Synergistic arsenic(V) and lead(II) retention on synthetic jarosite. I: Simultaneous structural incorporation behaviour and mechanism [J]. Environmental Science Processes & Impacts, 2018, 20(2): 354−369.

[15] GREY I E, SCARLETT N V Y, BRAND H E A. Crystal chemistry and formation mechanism of non-stoichiometric monoclinic K-jarosites [J]. Mineralogical Magazine, 2013, 77(3): 249−268.

[16] DUTRIZAC J E, JAMBOR J L. Jarosites and their application in hydrometallurgy [J]. Reviews in Mineralogy and Geochemistry, 2000, 40(1): 405−452.

[17] ASOKAN P, SAXENA M, ASOLEKAR S R. Recycling hazardous jarosite waste using coal combustion residues [J]. Materials Characterization, 2010, 61(12): 1342−1355.

[18] SHI Mei-qing, MIN Xiao-bo, KE Yong, LIN Zhang, YANG Zhi-hui, WANG Sheng, PENG Ning, YAN Xu, LUO Shuang, WU Jia-hui, WEI Yang-jin. Recent progress in understanding the mechanism of heavy metals retention by iron(oxyhydr) oxides [J]. Science of the Total Environment, 2021, 752: 141930.

[19] GUO Xiao-ru, YI Yong-guang, TAN Zhi-qiang, LIU Jing-fu. Environmentally relevant freeze-thaw cycles enhance the redox-mediated morphological changes of silver nanoparticles [J]. Environmental Science & Technology, 2018, 52(12): 6928−6935.

[20] WANG Li-qin, QI Yu-chun, DONG Yun-she, PENG Qin, GUO Shu-fang, HE Yun-long, LI Zhao-lin. Effects and mechanism of freeze-thawing cycles on the soil N_2O fluxes in the temperate semi-arid steppe [J]. Journal of Environmental

Sciences, 2017, 56(6): 192−201.
[21] LEHRSCH G A, SOJKA R E, CARTER D L, JOLLEY P M. Freezing effects on aggregate stability affected by texture, mineralogy, and organic matter [J]. Soil science Society of America Journal, 1991, 55(5): 1401−1406.
[22] O′CONCUBHAIR R, SODEAU J R. The effect of freezing on reactions with environmental impact [J]. Accounts of Chemical Research, 2013, 46(11): 2716−2724.
[23] JAHN L G, FAHY W D, WILLIAMS D B, SULLIVAN R C. Role of feldspar and pyroxene minerals in the ice nucleating ability of three volcanic ashes [J]. ACS Earth and Space Chemistry, 2019, 3(4): 626−636.
[24] LU Zhong-liang, XU Wen-liang, CAO Ji-wei, XIA Yuan-lin, DENG Qing-hua, LI Di-chen. Microstructures and properties of porous TiAl-based intermetallics prepared by freeze-casting [J]. Transactions of Nonferrous Metals Society of China, 2020, 30(2): 382−391.
[25] UTHRAKUMAR R, VESTA C, RAJ C J, KRISHNAN S, DAS S J. Bulk crystal growth and characterization of non-linear optical bisthiourea zinc chloride single crystal by unidirectional growth method [J]. Current Applied Physics, 2010, 10(2): 548−552.
[26] RAJAGOPALAN N R, KRISHNAMOORTHY P. Contemporary studies on growth and characterization of bis(thiourea) strontium chloride—A potential optoelectronic NLO material [J]. Optik, 2016, 127(7): 3582−3589.
[27] RAJAGOPALAN N R, KRISHNAMOORTHY P, JAYAMOORTHY K. A strategic approach to physico-chemical analysis of bis (thiourea) lead chloride—A reliable semi-organic nonlinear optical crystal [J]. Optics & Laser Technology, 2017, 89(2): 6−15.
[28] SONDI I, SHI S, MATIJEVIC′ E. Precipitation of monodispersed basic iron(III) sulfate (sodium jarosite) particles [J]. Colloid and Polymer Science, 2001, 279(2): 161−165.
[29] SZPACZYŃSKI J A, WHITE J A, CÔTÉ C L. Separation of contaminants in the freeze/thaw process [J]. Chemical and Process Engineering, 2017, 38(2): 249−264.
[30] SIVAKUMAR N, KANAGATHARA N, VARGHESE B, BHAGAVANNARAYANA G, GUNASEKARAN S, ANBALAGAN G. Structure, crystal growth, optical and mechanical studies of poly bis(thiourea) silver(I) nitrate single crystal: A new semi organic NLO material [J]. Spectrochimica Acta (Part A): Molecular and Biomolecular Spectroscopy, 2014, 118: 603−613.
[31] KIM K, KIM J, BOKARE A D, CHOI W, YOON H I, KIM J. Enhanced removal of hexavalent chromium in the presence of H_2O_2 in frozen aqueous solutions [J]. Environmental Science & Technology, 2015, 49(18): 10937−10944.
[32] JEONG D, KIM K, MIN D W, CHOI W. Freezing-enhanced dissolution of iron oxides: Effects of inorganic acid anions [J]. Environmental Science & Technology, 2015, 49(21): 12816−12822.
[33] ZHANG Ze, MA Wei, FENG Wen-jie, XIAO Dong-hui, HOU Xin. Reconstruction of soil particle composition during freeze-thaw cycling: A review [J]. Pedosphere, 2016, 26(2): 167−179.
[34] GERMAN S V, NOVOSELOVA M V, BRATASHOV D N, DEMINA P A, ATKIN V S, VORONIN D V, KHLEBTSOV B N, PARAKHONSKIY B V, SUKHORUKOV G B, GORIN D A. High-efficiency freezing-induced loading of inorganic nanoparticles and proteins into micron- and submicron-sized porous particles [J]. Scientific Reports, 2018, 8(1): 17763.
[35] MIN D W, KIM K, LUI K H, KIM B, KIM S, CHO J, CHOI W. Abiotic formation of humic-like substances through freezing-accelerated reaction of phenolic compounds and nitrite [J]. Environmental Science & Technology, 2019, 53(13): 7410−7418.
[36] KIM K, MENACHERRY S P M, KIM J, CHUNG H Y, JEONG D, SAIZ-LOPEZ A, CHOI W. Simultaneous and synergic production of bioavailable iron and reactive iodine species in ice [J]. Environmental Science & Technology, 2019, 53(13): 7355−7362.

硫脲冻融循环法分离硫酸铅–黄钠铁矾共沉淀物中的铅

彭 俊[1]，魏杨金[1]，史美清[1,2]，吴佳蕙[1]，王庆伟[1,2]，林 璋[1,2]，刘 恢[1,2]，颜 旭[1,2]

1. 中南大学 冶金与环境学院，长沙 410083；
2. 国家重金属污染防治工程技术研究中心，长沙 410083

摘 要：采用硫脲冻融循环法分离硫酸铅–黄钠铁矾共沉淀物中的铅。研究结果表明，在硫脲冻融循环过程中，共沉淀物中混杂的硫酸铅逐渐在黄钠铁矾表面聚集，同时通过冷冻浓缩作用促进硫酸铅与硫脲反应，形成硫脲铅(Pb-tu)新物相。随着冻融循环次数的增加，黄钠铁矾周围的硫酸铅不断转化为 Pb-tu，直至反应完全。12 次冻融循环后，黄钠铁矾和 Pb-tu 发生自发分层现象，即黄钠铁矾沉于底部，而 Pb-tu 浮在黄钠铁矾的上层，从而实现铅的分离。分离后黄钠铁矾沉淀的浸出毒性比分离前降低了 73.7%。本研究表明，硫脲冻融循环法在分离硫酸铅–黄钠铁矾共沉淀物中的铅和铁矾渣中有价金属回收方面具有较大的应用潜力。

关键词：铁矾渣；硫酸铅；冻融循环法；硫脲；分离

(Edited by Wei-ping CHEN)